Computer Fraud and Security
ISSN (online): 1873-7056

A Model for Muscle Injury Recovery after Training based on Computer Biomimetic Technology

XiaoFeng Hu

ChengDu Sport University, ChengDu, SiChuan, China

Abstract

In order to improve the recovery effect of muscle injury after high-intensity training of rope skipping, this paper combines computer bionics technology to study the muscle injury recovery after high-intensity training of rope skipping. Moreover, this paper explains the working principle of the bionic muscle by combining the bionic muscle model proposed in this paper, and analyzes several stress situations of the bionic muscle during work. In addition, the relationship between the pressure difference between the two ends of the piston and the velocity of the damping rod during the movement of the damping rod is obtained by analyzing the liquid flow in the damping hole on the piston. The simulation study shows that the method proposed in this paper can effectively improve the training injury recognition and recovery effect of high intensity training muscle model in rope skipping.

Keywords: rope skipping; high-intensity training; muscle injury; recovery; computer biomimetic technology

1.INTRODUCTION

In recent years, with the development of the Internet and the emergence of smart phones, various mobile exercise software can monitor the daily physical activity of the people. Smartphones are more accessible to the people than laboratory energy-consuming instruments and do not impose financial burdens on the wearer. Moreover, if the built-in acceleration sensor of the smartphone can effectively evaluate the fitness skipping exercise, it is bound to scientifically guide the public to perform the fitness skipping exercise. For this reason, it is necessary to use the built-in accelerometer of smartphones to establish an effective prediction equation for the exercise of fitness skipping, whether it is from the perspective of the accuracy of energy consumption assessment by the built-in accelerometer of smartphones or the gap between domestic and foreign related researches.

With the increasingly fierce competition and the continuous development of competitive sports, more and more science and technology are gradually being applied to sports research, and the application of sports biomechanics principles and methods in sports scientific research is no exception. It takes the theory and method of classical mechanics as the main application of modern science and technology, can objectively record the skills of athletes without affecting the normal training and competition of athletes, and can quickly feedback the research results to coaches and athletes. To better improve the technology provides important theoretical reference.

This paper combines computer bionics technology to study the recovery of muscle damage after high-intensity training of rope skipping, so as to improve the effect of high-intensity training of rope skipping and reduce the muscle damage of athletes.

2.RELATED WORK

The motion contraction is realized with the help of a special isokinetic load test device, which is that the load can be accurately adjusted with the joint movement process, that is to say, the load is the smallest at the weakest point of the joint angle tension, and the strongest at the joint angle tension. The point load is the maximum [1]. It can also be said that the tension produced by the muscle is always equal to the load in the joint range, and the muscle can contract at a constant speed or equivalent intensity. The isokinetic (isokinetic) muscle strength test is to measure the torque (torque curve) of the isokinetic muscle training technology and function at each angle of the tested link under the condition of a given selected range of motion and rotational speed. As an emerging technology, the test has been widely used in the research and clinical work of rehabilitation medicine and sports medicine. Because of its obvious advantages in terms of accuracy, safety and effectiveness, it is regarded as the

evaluation of muscle function. the golden method [2]. The isokinetic test method first originated in the United States in the 1960s, and has been widely used in Germany, Sweden, the United Kingdom, Japan, the Soviet Union and other countries. accepted by players and athletes. There are also many kinds of isokinetic testing instruments[3].

The clinical manifestations of muscle injury are mainly delayed muscle soreness after strenuous exercise, decreased muscle strength, decreased joint range of motion, and increased blood creatine kinase levels [4]. Symptoms generally appear a few hours after exercise and peak at 24-48 hours. The symptoms will resolve on their own in about a week until they disappear. The location of muscle soreness and tenderness is mainly the junction of the muscle belly at the distal end of the muscle, but in severe cases, the pain extends almost to the entire muscle belly[5]. DOMS is a well-known phenomenon to athletes. Although DOMS can heal itself, it may also cause other injuries to the trainer due to its long duration, which will seriously affect normal training and competition. For a long time, it has been a subject of sports medicine. One of the research hotspots in the field. Regarding the mechanism of DOMS, hypotheses such as mechanical injury, tissue inflammation, muscle spasm ischemia, and free radical damage have been proposed. At present, it seems that these mechanisms play their respective roles in different stages of DOMS [6]. According to these mechanism hypotheses, researchers have tried numerous treatments, including hot and cold therapy, anti-inflammatory drugs, massage, acupuncture, ultrasound therapy, etc., to alleviate the symptoms of DOMS and accelerate its recovery, but no simple, safe, Effective and satisfactory treatment[7].

During muscle contraction, mechanical force is transmitted from the myofibrils through the intracellular skeleton to the cell membrane and extracellular matrix, and then to the tendons and bones through the perimysium. During centrifugal exercise, the muscle cell membrane and the connective tissue around the cell will be repeatedly elongated under high tension, which may cause some collagen fibers to break and the cell membrane to be slightly damaged. Studies have shown that after eccentric exercise in rats, the muscle cell membrane is indeed damaged, and the proportion of muscle fibers with plasma membrane damage exceeds 20%. Abnormal muscle cell membrane permeability can lead to the loss of intracellular proteins (such as creatine kinase), changes in cell and tissue osmotic pressure, and a large amount of calcium ions entering the cell, resulting in a series of delayed reactions[8].

The disruption of sarcomere and exoskeleton proteins may be an important factor leading to the ultrastructural changes of muscle fibers [9]. Reference[10] used indirect immunofluorescence to show the cytoskeleton component desmin (desmin), and found that the myofibrillar cytoskeleton was blocked after centrifugal exercise, accompanied by increased autolysis. The studies in the literature [11] all show that the degradation of muscle desmin is increased and the expression is decreased in the early stage of exercise-induced muscle injury. Literature [12] found that after eccentric contraction, myosin (myosin) detached from the middle position of the sarcomere, and was closer to the Z line on one side. Since titin (titin) is involved in maintaining the normal position of myosin, this It may be due to the degradation or fragmentation of titin due to eccentric exercise.

Many studies have shown that a large amount of free radicals are produced in the body after strenuous exercise. Literature [13] directly measured free radicals by electron rotation resonance spectroscopy, and found that after strenuous exercise, the free radicals in rat skeletal muscle increased significantly. Reference [14]used the fluorescent probe method to detect free radicals in rat skeletal muscle after strenuous exercise, and obtained the same result. After strenuous exercise, the generation mechanisms of free radicals mainly include mitochondrial mechanism, xanthine oxidase mechanism, and neutrophil mechanism. Literature[15] proved that the mitochondrial respiratory chain produces oxygen free radicals. Reference [16] used chemiluminescence detection method to observe that the production of superoxide anion in skeletal muscle mitochondria was significantly increased after exhaustive exercise in rats. Major source of endogenous free radicals. In the process of catalyzing the oxidation of hypoxanthine and xanthine by xanthine oxidase, superoxide anion is formed. During strenuous exercise, skeletal muscle is relatively hypoxic, ATP is consumed in large quantities, and a large amount of hypoxanthine is produced in muscle tissue. At the same time, xanthine oxidase changes from a reduced form to an oxidized form. It can oxidize hypoxanthine to increase the generation of superoxide anion [17]. Evidence has shown that after strenuous exercise, the concentration of hypoxanthine and its oxidation

product uric acid in skeletal muscle and blood increases significantly [18], and the activity of xanthine oxidase in blood also increases significantly[19].

3.BIOMECHANICAL MODEL OF SKELETAL MUSCLE

From a macroscopic point of view, the mechanical properties of the muscle are related to the length of the muscle itself, the speed of contraction, and the external stimulation. Since the 20th century, many scholars at home and abroad have carried out a lot of experiments on muscles, achieved a lot of results, and established many simplified models of muscles.

When one end of the muscle is loosened, its tension becomes T, and the contraction velocity V of the muscle fiber is measured, and the original length of the muscle is recorded as L_0. The famous Hill equation is:

$$(a+T)(V+b)=b(T_0+a) \quad (1)$$

In the formula, a and b are both constants.

The Hill equation contains three independent constants a、b、T_0.

The Hill equation can also be written as:

$$v=b\frac{T_0-T}{T+a} \quad (2)$$

It can be known from the above formula that when T=0, v can reach the maximum value, and at this time $v=b\frac{T_0}{a}$.

The comparison graph of Hill equation and experimental results is shown in Figure 1.

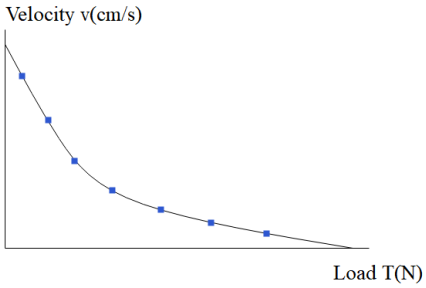

Fig. 1 Comparison of T and v data of isotonic contraction measured in the experiment and Hill's equation

Based on the function of skeletal muscle, a functional model of skeletal muscle is established as shown in Figure 2(a), where CE is the contractile unit and SE is the tandem unit. After that, a three-element model of skeletal muscle was established, as shown in Figure 2(b), where PE is a parallel elastic element.

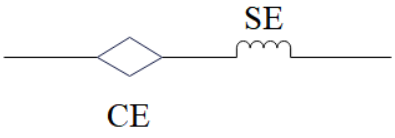

(a) Hill two-element model of skeletal muscle

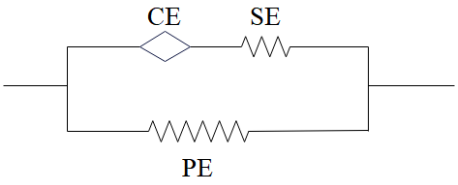

(b) Three-element model of skeletal muscle

Figure 2 Elemental model of skeletal muscle

Hill's two-element model has the following features:

$$\begin{cases} L = L_s + L_c \\ T = T_c = T_s \end{cases} \quad (3)$$

In the above formula, L is the muscle length, T is the muscle tension, S is the series elastic unit, and C is the contractile unit.

The geometric representation of skeletal muscle elements is shown in Figure 3.

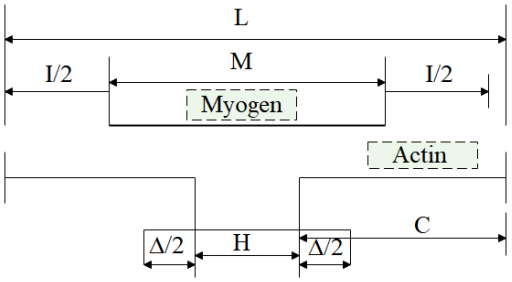

Figure 3 Geometric representation of the elements of the iliac muscle

In Figure 3, M is the length of myosin fibers, c is the length of actin fibers, △ is the length of the overlapping portion of myosin and actin, H and I are the widths of the H-band and I-band, and L is the total length of muscle fibers.

At the same time, the basic dynamic equation of the muscle is obtained:

(1) Under isometric contraction

$$\frac{d\tau}{dt} = \left(\frac{\partial S}{\partial \eta}\Big|_{\Delta} + \frac{\partial S}{\partial \Delta}\Big|_{\eta}\right)\frac{d\Delta}{dt} \quad (4)$$

(2) Under isotonic contraction

$$\left(\frac{dP}{dL} + \frac{\partial S}{\partial \eta}\Big|_{\Delta}\right)\frac{dL}{dt} + \left(\frac{\partial S}{\partial \eta}\Big|_{\Delta} + \frac{\partial S}{\partial \Delta}\Big|_{\eta}\right)\frac{d\Delta}{dt} = 0 \quad (5)$$

In the formula, τ is the total stress of the sarcomere, η is the elongation of the series elastic element, S is the stress function of the series elastic element, and P is the stress function of the parallel elastic element.

The constitutive model describing the change of skeletal muscle length from the microscopic aspect, the model of the muscle is shown in Figure 46. This model is called the Huxley model.

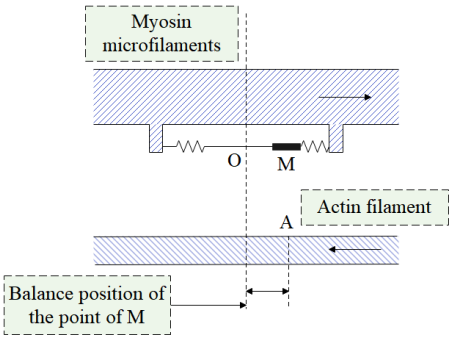

Figure 4 Huxley model

Four assumptions are made:

(1) The function of each transverse bridge is independent;

(2) At any time, there is a high probability that the transverse bridge will only bind to the nearest actin;

(3) The distance from the cross bridge to the nearest junction has a constant probability density;

(4) Each transverse bridge is elastically linked to actin, and when the transverse bridge is not bound to actin, it performs continuous thermodynamic free motion near an undefined equilibrium position.

The slip rate equation is:

$$\left[\frac{\partial n}{\partial t}\right] - v(t)\left[\frac{\partial n}{\partial t}\right] = \dot{f}(1-n) - g \cdot n \quad (6)$$

In cross section, the force acting on the myofilament is:

$$p(t) = \frac{mskA}{2l}\int_{-\infty}^{+\infty} n\,(x,t)xdx \quad (7)$$

$$K_C = \frac{\Delta p}{\Delta X} = \left(\frac{ms^2k}{2l}\right)\left(\frac{A}{2X}\right)\int_{-\infty}^{+\infty} n\,(x,t)dx \quad (8)$$

In the above formulas, $v(t)$ is the sliding velocity of the myofilament, fg is the function of the binding rate of the transverse bridge, and m is the density of the myofilament per unit volume, A is the cross-sectional area, s is the length of the sarcomere, k is the elastic coefficient of the transverse bridge, and $n(x,t)$ is the binding rate of the transverse bridge.

The rheology is based on the Huxley model, and its comparative model is shown in Figure 5.

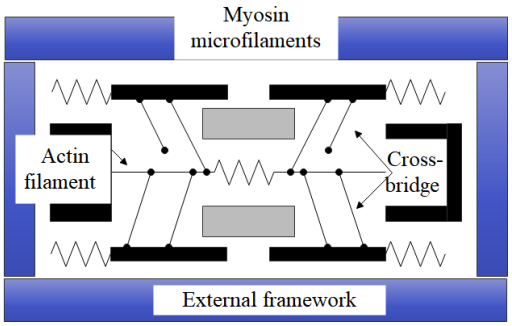

a Physical model base on Huxley

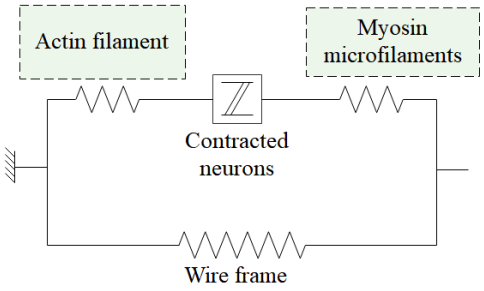

b rheological model of the b-derived skeletal muscle

Figure 5 Mechanical model of the muscle

The difference between the rheological model and the Huxley model is that the inherent elasticity of all muscle filaments is considered, while the rheological model replaces the motion behavior of the transverse bridge with linear contractile elements.

The three-dimensional mathematical model of the length-velocity-load of a single muscle is obtained by collecting various parameters such as the length, speed and load of the muscle during the muscle contraction process, and the contraction speed is regarded as a function of the muscle length and load. The expression of this function is as follows:

$$V(l,m) = K_v(l - L_p)(L_a - l)\,exp\left[\frac{m(l-L_p)}{K_m}\right] \quad (9)$$

In the formula, $L_a < l < L_p, m$ is the load mass, 1 is the instantaneous length of the muscle flash, K_v is the velocity constant, L_p is the passive maximum equilibrium length when the load is m, L_a is the active minimum length when the mass is m, and K_m is the mass coefficient of the muscle. Among the above parameters, K_v is related to the maximum contraction speed of the muscle in the contraction range, L_a、L_p is obtained from the length-load relationship of the muscle, and K_m is obtained from the linear regression of the experimental data.

Based on the Hill three-element model, this paper proposes a mechanical model to realize the Hill three-element. The model is shown in Figure 6.

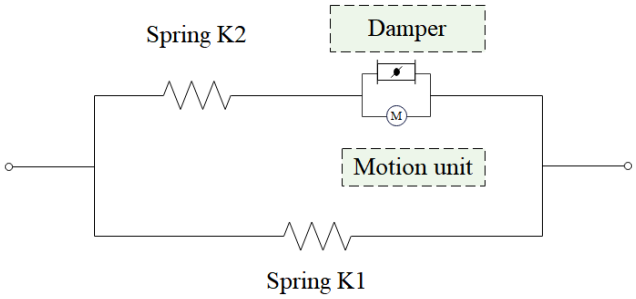

Figure 6 Principle of bionic muscle

We set the contraction length of the bionic muscle to be X, the damping coefficient of the damper to be C, and the force of the series system part to be F2. For the series system part, we can get:

$$\frac{dX}{dt} = \frac{d\frac{F_2}{K_2}}{dt} + \frac{F_2 - F_{AE}}{C} = \frac{1}{K_2}\frac{dF_2}{dt} + \frac{F_2 - F_{AE}}{C} \quad (10)$$

If the partial force of the parallel system is set as F_1, we can get:

$$F_1 = K_1 \cdot X \quad (11)$$

The external pulling force of the bionic muscle is $F = F_1 + F_2$.

For formula (10), we can get:

$$\frac{dX}{dt} = \frac{1}{K_2}\frac{d(F - F_1)}{dt} + \frac{F - F_1 - F_{AE}}{C} \quad (12)$$

Bringing formula (11) into formula (12) and arranging the formula, we can get:

$$\left(1 + \frac{K_1}{K_2}\right)\frac{dX}{dt} + \frac{K_1}{C}X = \frac{1}{K_2}\frac{dF}{dt} + \frac{F}{C} - \frac{F_{AE}}{C} \quad (13)$$

When $R = \frac{C}{K_2}$, formula (13) becomes:

$$(K_1 + K_2)\frac{dX}{dt} + \frac{K_2}{R}X = \frac{dF}{dt} + \frac{F}{R} - \frac{F_{AE}}{R} \quad (14)$$

Formula (14) is the constitutive equation of this bionic muscle.

In this paper, the bionic muscle is designed according to the Hill three-element model, and its principle is shown in Figure 7. The motion pair of the cylinder piston in the figure represents the damper, which forms an active contraction unit under the action of the driving force F, which plays the role of driving the bionic muscle contraction. The active contraction unit is connected in series with the spring K2, and then in parallel with the spring K1.

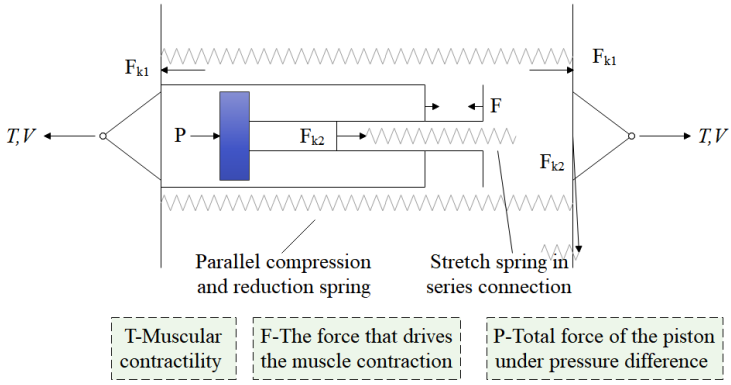

Figure 7 The working principle of the bionic muscle

In order to make this bionic muscle imitate the motion pattern of human muscle, it is required that the bionic muscle can contract under the action of the driving force F. At this time, the two ends connected to the motion system will generate tension T and motion speed V, and the parallel spring will compress and store energy.

According to the above requirements, the overall model of the bionic muscle designed in this paper is shown in Figure 8.

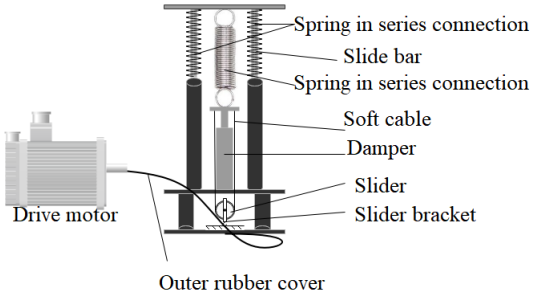

Figure 8 Bionic muscle model

This bionic muscle works in two ways. Through the force analysis of the bionic muscle work, the control conditions are provided for designing the length and stiffness of the springs K1 and K2.

(I) When the driving force F is zero, according to the movement conditions of both ends of the bionic muscle, this situation can be divided into two types.

(1) The bionic muscle is in a resting state, that is, the tension T and velocity v at both ends of the bionic muscle are zero, and the piston does not move. At this time, the resting length is l_0, and $T = F_{k2} - F_{kl} = 0$ is obtained from the pulling force $F_{k2} = F_{k1}$.

(2) The bionic muscle is in a passive tension state, that is, the tension T and velocity v at both ends of the bionic muscle are not zero, and the piston movement tends to return to the initial position or at the initial position.

(II) When the driving force F is not zero. Generally, T is not zero, and the two extreme cases are T=0 or v=0. According to the movement conditions of both ends of the bionic muscle, it is divided into the following three situations.

(1) $T > 0, v > 0$. It shows that the bionic muscle provides tension in the motor system, and the contraction speed is coordinated with the motor system. The muscle tension at this time is $T = Fk2 - Fk1 > 0$. For the piston, there is $P(v) + Fk2 = F$.

(2) $T > 0, v = 0$. It shows that the bionic muscles provide pulling force in the movement system and support the static balance of the movement system. The muscle tension at this time is $T = \mathrm{Fk2} - \mathrm{Fk1} > 0$. For the piston, there is $P(v) = 0, Fk2 = F$.

(3) v<0. It indicates that the muscle is passively elongated in the motor system, and F is smaller.

The initial length of the entire bionic muscle is designed to be 316mm. It can contract 10% of its total length, that is, 31mm, through the self-excitation of the muscle under no-load conditions. When it is fully contracted, the internal stress generated by the muscle is 509N. The parameters of the bionic muscle are shown in Figure 9, 1_1 is the length of the bionic muscle, F_C is the damping force provided by the damper, and F_A is the excitation force of the muscle, F_2 is the elastic force provided by spring K_2, and F_1 is the elastic force provided by spring K_1.

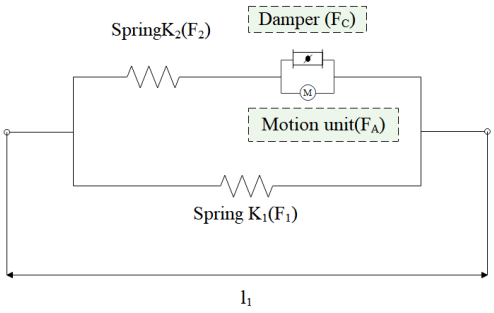

Figure 9 Biomimetic muscle parameters

The rectus femoris contracts 31mm, so there is:

$$\Delta l\, max = \Delta l \mathrm{mm} 2 max cmax_{1max}$$

Among them, $\Delta 1$ is the contracted length of the bionic muscle, Δl_1 is the contracted length of the spring k_1, Δl_c is the contracted length of the damper, and Δl_2 is the extended length of the spring K_2.

When the bionic muscle is fully contracted, there is:

$$T = F_{K1} - F_{K2} = 509N$$

According to the analysis, when the contraction ratio of spring K_1 and K_2 reaches 1:1, the overall properties of the bionic muscle are the best. Therefore, we design:

$$\Delta l \mathrm{mm}_{1max}$$

$$\Delta l \mathrm{mm}_{2max}$$

From formula (12), we can get:

$$\Delta lc \mathrm{mm}_{max}$$

Based on the above design parameters, there is:

$$31 \times K_2 - 31 \times K_1 = 509.2N$$

The elastic coefficients of the springs are all integer values, so the elastic coefficient of the spring K_1 is $20N/\mathrm{mm}$, and the elastic coefficient of the spring K_2 is $36N/\mathrm{mm}$.

It can be seen from the previous that the spring is $K_2 = 36N/\mathrm{mm}$, and the maximum tensile length of the spring is 31mm. From this, it can be known that the maximum tensile force borne by the spring K_2 is:

$$F_2 = 36 \times 31 = 1116N$$

Because the spring works under the general load, according to the third type of spring, the carbon spring grade C is selected. The ultimate load for the initial work is:

$$P_{j'} = F_2/0.8 = 1116/0.8 = 1395N$$

When choosing a spring, there is $P_j > P_{j'}$. By consulting the relevant information of spring design, we choose the spring material diameter as d=6mm, the middle diameter as D=30mm, the allowable stress of the material as

$T = 710\text{MPa}$, the working limit load as $P_j = 1530N$, the single-turn deformation under the working limit load as $f_j = 3.320\text{mm}$, and the single-turn stiffness as $P_d^{'} = 471N/\text{mm}$.

The effective number of turns of the spring is:

$$n = P_d^{'}/P^{'} = 471/36 = 13.08$$

We take n=13.

The spring stiffness $K_2{}^{'}$ is:

$$K_2{}^{'} = 471/13 = 36.2N/\text{mm}$$

The amount of deformation under the working limit load is:

$$F_j = 13 \times 3.320 \times 0.8 \approx 34.5\text{mm}$$

The outer diameter D_2 of the spring is:

$$D_2 = D + d = 30 + 6 = 36\text{mm}$$

The inner diameter D_1 of the spring is:

$$D_1 = D + d = 30 - 6 = 24\text{mm}$$

The free length H_0 is:

$$H_0 = (n + 1.5)d + 2D = 147\text{mm}$$

Considering the force balance of the whole system, so that it is not affected by the rotational moment, two parallel springs are designed, the stiffness of each spring is $10N/\text{mm}$, and the maximum compression length is 31mm. From this, it can be known that the maximum tensile force F_1 that the spring K_1 bears is:

$$F_1 = 10 \times 31 = 310N$$

The working limit load of each parallel spring is:

$$P_{j'} = 1.25F1 = 387.5N$$

By consulting the relevant information of spring design, we choose the spring material diameter as d=3.5mm, the middle diameter as D=18mm, the allowable stress of the material as T=785MPa, the working limit load as $P_j = 564.41N$, the single-turn deformation under the working limit load as $f_j = 2.221\text{mm}$, and the single-turn stiffness as $P_{d_d} = 254N/\text{mm}$.

The effective number of turns of the spring:

$$n = P_d^{'}/P^{'} = 254/10 = 25.4$$

We take n=25.

The total number of spring turns is:

$$n_1 = 25 + 2 = 27$$

The spring stiffness K_2 is:

$$K_{2'} = 254/25 = 10.16N/\text{mm}$$

The amount of deformation under the working limit load is:

$$F_j = 10 \times 2.221 = 22.21\text{mm}$$

The pitch t is:

$$t = F_j/n + d = 22.21/25 + 3.5 = 4.39\text{mm}$$

The outer diameter D_2 of the spring is:

$$D_2 = D + d = 18 + 3.5 = 21.5\text{mm}$$

The outer diameter D_1 of the spring is:

$$D_1 = D - d = 18 - 3.5 = 14.5\text{mm}$$

The free length H_0 is:

$$H_0 = nt + 1.5d = 115\text{mm}$$

Fig. 10 is a sectional view of the piston and the sleeve. We set the velocity and pressure at the inlet section 1-1 of the orifice to be v_1, P_1, respectively, the velocity and pressure at the section 2-2 of the orifice to be v_2、P_2, respectively, and the velocity and pressure at the downstream outlet section x-x to be v_x、P_x, respectively. The velocity and pressure at the section s-s of the upstream inlet body are $v_{S\ and\ P_S}$, respectively, $, d$ and D are the diameters of the damping hole and the cylinder block, D_1 is the diameter of the piston guide rod, and n is the number of damping holes. It is assumed here that the hydraulic oil is purely viscous, that is, the hydraulic oil is a Newtonian fluid, and the flow of the hydraulic oil in the orifice is laminar. At the same time, the flow velocity of hydraulic oil in the damping hole is v, then there is $v_1 = v_2 = v$.

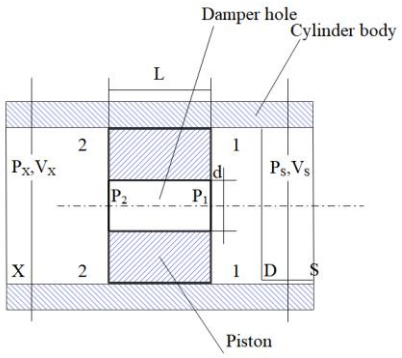

Figure 10 Schematic diagram of the cross section of the damping hole

From the Bernoulli equation, the equations of section s-s and section 1-1 can be obtained as:

$$\frac{P_S}{\rho g} + \frac{a_S v_S^2}{2g} = \frac{p_1}{\rho g} + \frac{aV_1^2}{2g} + \zeta_1 \frac{V_1^2}{2g} \quad (15)$$

In the formula, a_s, a is the kinetic energy correction coefficient at the s-s section and the 1-1 section respectively, ρ is the hydraulic oil density, and ζ_1 is the local resistance coefficient at the inlet. Since the flow velocity distribution at 1 is uniform, there is a = 1.

It can be obtained by the momentum theorem:

$$\rho Q(\beta_2 v - \beta_x v_x) = (p_x - p_2)A_x \quad (16)$$

In the formula, β_2, β_x is the kinetic energy correction coefficient, Q is the flow through the orifice, and A_x is the cross-sectional area of the section x-x.

According to formulas (15) and (16), the pressure difference between section s-s and section x-x is obtained as:

$$\Delta P = P_S - P_x = P_1 + (1 + \zeta_1)\rho \frac{v^2}{2} - \rho \frac{a_S v_S^2}{2} - P_2 - \rho V_x(\beta_2 v - \beta_x v_x) \quad (17)$$

The fluid continuity equation of the section s-s and the piston section 1-1 can be obtained according to the continuity equation of the fluid:

$$\pi \left(\frac{D^2 - D_1^2}{4}\right) V_S = n\pi \left(\frac{d}{2}\right)^2 v \quad (18)$$

We set $m^2 = \frac{nd^2}{D^2 - D_1^2}$.

Therefore, there is:

$$v_S = v_x = m^2 v \quad (19)$$

By formula (17) (18) (19), it can be obtained:

$$\Delta P = P_S - P_x = P_1 - P_2 + [1 + \zeta_1 - a_S m^4 - 2m^2(\beta_2 - \beta_x m^2)]\rho\frac{v^2}{2} \quad (20)$$

From the literature, we can get:

$$\Delta P' = \frac{32\mu l v}{d^2} + k\rho\frac{v^2}{2} + \zeta_2\rho\frac{v^2}{2} \quad (21)$$

In the formula, $\Delta P'$ is the pressure difference between section 1-1 and section 2-2, v is the fluid velocity in the orifice, and l is the length of the orifice. k generally takes 1.30. Substituting formula (21) into (20), we can get:

$$\Delta P = P_s - P_x = \frac{32\mu l v}{d^2} + [(\zeta_1 + \zeta_2 + k + 1) - a_S m^4 - 2m^2(\beta_2 - \beta_x m^2)]\rho\frac{v^2}{2} \quad (22)$$

Since $D^2 - D_1^2$ is much larger than h, the higher-order quantities of m are ignored. We set $\xi = 1 + k$, so that we can get:

$$\Delta P = \frac{32\mu l v}{d^2} + (\xi + \zeta_1 + \zeta_2)\rho\frac{v^2}{2} \quad (23)$$

The damping force is:

$$F = A\Delta P = \pi\left(\frac{D^2 - D_1^2}{4}\right)\left(\frac{32\mu v}{d^2} + (\xi + \zeta_1 + \zeta_2)\rho\frac{v^2}{2}\right) \quad (24)$$

Formula (24) reflects the relationship between the damping force and the flow velocity in the orifice, and what we need is the relationship between the damping force and the piston motion, so it needs to be converted. Substituting formula (28) into formula (24), we have:

$$F = A\Delta P = \frac{8\pi(D^2 - D_1^2)^2\mu l v_s}{nd^4} + \frac{\pi\rho(D^2 - D_1^2)^3 v_S^2}{8n^2 d^4}[(\xi + \zeta_1 + \zeta_2)] \quad (25)$$

We set the speed of the piston to be v, the damper is sealed, and $v = v_s$, then formula (25) can be written as the following form:

$$F = A\Delta P = \frac{8\pi(D^2 - D_1^2)^2\mu l v}{nd^4} + \frac{\pi\rho(D^2 - D_1^2)^3 v^2}{8n^2 d^4}[(\xi + \zeta_1 + \zeta_2)] \quad (26)$$

In the formula, F is the damping force provided by the damping hole, and A is the difference between the cross-sectional area of the cylinder block and the cross-sectional area of the guide rod. It can be seen from the reference materials that the square term of v can be ignored when the vibration frequency of the system is small, so the damping force and the speed of the piston can be written as the following relationship:

$$F = \mathrm{CV}$$

C in the formula is the damping coefficient.

$$C = \frac{8\pi(D^2 - D_1^2)^2\mu l}{nd^4} \quad (27)$$

The above formula C is the calculation formula of the damping coefficient. C is related to the geometric characteristics of the piston and the small hole, and the fluid viscosity coefficient, which provides a theoretical basis for the selection and customization of the damper.

RESULTS

Research on muscle injury recovery after high-intensity training of rope skipping

Combined with the simulation algorithm in the third part, the high intensity training muscle model in rope skipping proposed in this paper is shown in Figure 11.

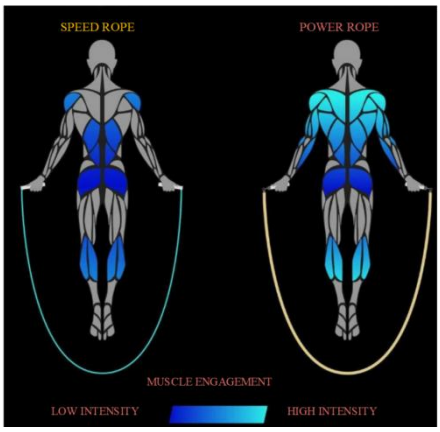

Figure 11 High intensity training muscle model in rope skipping

Combined with the bionic model in the third part, the training damage recognition and recovery effects of the high intensity training muscle model in rope skipping are evaluated, and the results shown in Tables 1 and 2 are obtained.

Table 1 Training injury recognition of high intensity training muscle model in rope skipping

Damage identification	NUM	Damage identification	NUM	Damage identification	NUM	Damage identification
90.23	15	87.01	29	88.48	43	90.71
91.21	16	87.47	30	89.86	44	87.46
88.87	17	92.80	31	86.30	45	84.31
88.90	18	87.06	32	88.13	46	86.09
88.40	19	84.11	33	90.89	47	85.96
84.38	20	92.05	34	89.34	48	92.84
91.23	21	86.02	35	88.51	49	90.45
87.75	22	89.21	36	89.95	50	86.60
88.05	23	85.96	37	92.68	51	84.79
92.98	24	88.43	38	92.40	52	84.59
85.81	25	92.55	39	87.62	53	91.61
90.18	26	91.62	40	84.25	54	92.62
90.26	27	88.70	41	91.25	55	85.13
90.59	28	85.04	42	86.05	56	85.25

Table 2 Recovery effect of high intensity training muscle model in rope skipping

NUM	Restoration effect	NUM	Restoration effect	NUM	Restoration effect	NUM	Restoration effect
1	83.72	15	84.86	29	83.54	43	88.14
2	79.79	16	88.45	30	78.46	44	85.45
3	86.94	17	86.75	31	84.54	45	81.21
4	88.42	18	79.00	32	78.55	46	84.79

5	84.76	19	84.59	33	81.11	47	88.39
6	79.26	20	79.05	34	87.12	48	86.84
7	81.92	21	88.24	35	79.86	49	83.30
8	83.86	22	79.47	36	87.29	50	85.76
9	84.43	23	82.00	37	83.04	51	85.17
10	79.97	24	78.85	38	82.08	52	83.94
11	86.69	25	79.66	39	86.08	53	88.38
12	87.21	26	80.07	40	79.84	54	78.60
13	83.09	27	87.75	41	80.53	55	78.92
14	82.67	28	86.12	42	84.29	56	82.61

4. CONCLUSION

From the above simulation studies, it can be seen that the method proposed in this paper can effectively promote the training damage identification and recovery effect of high intensity training muscle model in rope skipping.

As a national fitness program that is easy to learn, relatively rich in content, and requires very little equipment on the site, rope skipping can improve the strength of the upper and lower limbs, cardiopulmonary capacity, and physical coordination. At the same time, it can effectively reduce stress and relieve emotions for modern people, and the benefits to the body are obvious. Even many foreign medical experts call skipping rope "the most perfect exercise". This paper combines computer bionics technology to carry out research on muscle injury recovery after high-intensity training of rope skipping. The simulation study shows that the method proposed in this paper can effectively promote the training injury recognition and recovery effect of high intensity training muscle model in rope skipping.

REFERENCES

[1] XU, J., TASAKA, K., & YAMAGUCHI, M. (2021). Fast and Accurate Whole-Body Pose Estimation in the Wild and Its Applications. ITE Transactions on Media Technology and Applications, 9(1), 63-70.

[2] Szűcs, G., & Tamás, B. (2018). Body part extraction and pose estimation method in rowing videos. Journal of computing and information technology, 26(1), 29-43.

[3] Gu, R., Wang, G., Jiang, Z., & Hwang, J. N. (2019). Multi-person hierarchical 3d pose estimation in natural videos. IEEE Transactions on Circuits and Systems for Video Technology, 30(11), 4245-4257.

[4] Nasr, M., Ayman, H., Ebrahim, N., Osama, R., Mosaad, N., & Mounir, A. (2020). Realtime Multi-Person 2D Pose Estimation. International Journal of Advanced Networking and Applications, 11(6), 4501-4508.

[5] Thành, N. T., & Công, P. T. (2019). An Evaluation of Pose Estimation in Video of Traditional Martial Arts Presentation. Journal of Research and Development on Information and Communication Technology, 2019(2), 114-126.

[6] Petrov, I., Shakhuro, V., & Konushin, A. (2018). Deep probabilistic human pose estimation. IET Computer Vision, 12(5), 578-585.

[7] Hua, G., Li, L., & Liu, S. (2020). Multipath affinage stacked—hourglass networks for human pose estimation. Frontiers of Computer Science, 14(4), 1-12.

[8] Aso, K., Hwang, D. H., & Koike, H. (2021, February). Portable 3D Human Pose Estimation for Human-Human Interaction using a Chest-Mounted Fisheye Camera. In Augmented Humans Conference 2021 (pp. 116-120).

[9] Mehta, D., Sridhar, S., Sotnychenko, O., Rhodin, H., Shafiei, M., Seidel, H. P., ... & Theobalt, C. (2017). Vnect: Real-time 3d human pose estimation with a single rgb camera. ACM Transactions on Graphics (TOG), 36(4), 1-14.

[10] Liu, S., Li, Y., & Hua, G. (2018). Human pose estimation in video via structured space learning and halfway temporal evaluation. IEEE Transactions on Circuits and Systems for Video Technology, 29(7), 2029-2038.

[11] Ershadi-Nasab, S., Noury, E., Kasaei, S., & Sanaei, E. (2018). Multiple human 3d pose estimation from multiview images. Multimedia Tools and Applications, 77(12), 15573-15601.

[12] Nie, X., Feng, J., Xing, J., Xiao, S., & Yan, S. (2018). Hierarchical contextual refinement networks for human pose estimation. IEEE Transactions on Image Processing, 28(2), 924-936.

[13] Nie, Y., Lee, J., Yoon, S., & Park, D. S. (2019). A Multi-Stage Convolution Machine with Scaling and Dilation for Human Pose Estimation. KSII Transactions on Internet and Information Systems (TIIS), 13(6), 3182-3198.

[14] Zarkeshev, A., & Csiszár, C. (2019). Rescue Method Based on V2X Communication and Human Pose Estimation. Periodica Polytechnica Civil Engineering, 63(4), 1139-1146.

[15] McNally, W., Wong, A., & McPhee, J. (2018). Action recognition using deep convolutional neural networks and compressed spatio-temporal pose encodings. Journal of Computational Vision and Imaging Systems, 4(1), 3-3.

[16] Díaz, R. G., Laamarti, F., & El Saddik, A. (2021). DTCoach: Your Digital Twin Coach on the Edge During COVID-19 and Beyond. IEEE Instrumentation & Measurement Magazine, 24(6), 22-28.

[17] Bakshi, A., Sheikh, D., Ansari, Y., Sharma, C., & Naik, H. (2021). Pose Estimate Based Yoga Instructor. International Journal of Recent Advances in Multidisciplinary Topics, 2(2), 70-73.

[18] Colyer, S. L., Evans, M., Cosker, D. P., & Salo, A. I. (2018). A review of the evolution of vision-based motion analysis and the integration of advanced computer vision methods towards developing a markerless system. Sports medicine-open, 4(1), 1-15.

[19] Bhombe, J., Jethwa, A., Singh, A., & Nagarhalli, T. (2021). Review of Pose Recognition Systems. VIVA-Tech International Journal for Research and Innovation, 1(4), 1-8.